Seismic characteristics of the 2022-2023 unrest episode at Taupō volcano, Aotearoa New Zealand

Oliver D. Lamb [*1], Stephen Bannister [2], John Ristau [2], Craig Miller [1], Steve Sherburn [1], Katie Jacobs [2], Jonathan B. Hanson [2], Elisabetta D'Anastasio [2], Sigrún Hreinsdóttir [2], Eveanjelene Snee [2], Mike Ross [2], Eleanor R. H. Mestel [3], Finnigan Illsley-Kemp [3]

[1]Te Pū Ao | GNS Science, Wairakei Research Centre, Taupō, 3384, New Zealand, [2]Te Pū Ao | GNS Science, Avalon Campus, Lower Hutt, 5010, New Zealand, [3]Te Kura Tātai Aro Whenua School of Geography, Environment and Earth Sciences, Te Herenga Waka Victoria University of Wellington, PO Box 600, Wellington, 6140, New Zealand

Abstract   Taupō is a large caldera volcano located beneath a lake in the centre of the North Island of New Zealand and most recently erupted ∼1800 years ago. The volcano has experienced at least 16 periods of unrest since 1872, each of which was characterised by increased seismic activity. Here we detail seismic activity during the most recent period of unrest from May 2022 to May 2023. The unrest was notable for the highest number of earthquakes detected during instrumented unrest episodes, and for one of the largest magnitude earthquakes detected beneath the lake for at least 50 years (M_L 5.7). Relocated earthquakes indicate seismic activity was focused around an area hosting overlapping caldera structures and a hydrothermal system. Moment tensor inversion for the largest earthquake includes a non-negligible inflationary isotropic component. We suggest the seismic unrest was caused by the reactivation of faults due to an intrusion of magma at depth.

Tuhinga Whakarāpopoto   (te reo Māori) He ahi tipua oumu a Taupō e takoto ana i raro i te moana kei te pito tonu o Te Ika a Māui, tana pahūtanga hou o nā tata nei ∼ ko te 1800 tau ki muri. Mai i te tau 1872 16 ngā ngunguru a te ahi tipua, he mea tohu e te whakapikinga o te mahi rū. I rongonui ai mō te nui rawa o ngā rū i rangona i te wā e aroturukihia ana ngā wāhanga ngunguru e te pūrere, waihoki, mō te rū kaha rawa atu i rangona i raro i te moana mō te rima tekau tau neke atu kua hipa ake nei (M_L 5.7). E tohu ana ngā rū nekeneke ko te aronga o te rū ko tētahi wāhi whai hanga ouma e inaki ana tētahi i tētahi me tōna pūnaha puia. Kei te kōarotanga papatau pūmau mō te tino rū ko te wae ngotangota whakamakoha nui. E huatau ana mātou ko te puehu i tutu ai e te rū he mea ahu mai i te hohenga anō o ngā hapa i te whakaekenga hohonu iho o te tokarewa.

Non-technical summary   Taupō is a large volcano beneath a lake in New Zealand and has not erupted for over 1800 years. Since 1872, the volcano has had frequent episodes of unrest marked by higher numbers of earthquakes. Here we describe and analyse earthquakes detected during the most recent unrest episode from May 2022 to May 2023. This episode was the most intense observed in recent monitored history with the largest number of earthquakes as well as one of the largest magnitude earthquakes ever recorded beneath the lake. Our analysis suggests the unrest was caused by new magma entering the volcanic system causing earthquakes on faults associated with previous caldera collapse.

1   Introduction

Volcano observatories are tasked with monitoring and understanding volcanic unrest as well as communicating future scenarios to affected parties (e.g. emergency management personnel, local residents, and local to national governments). To help understand the current state of volcanic activity, historical information is needed regarding the frequency, severity and evolution of unrest or eruptive activity. This is a particular challenge for caldera volcanoes where modern day measurements may extend back several decades but do not capture a wide range of possible eruption scenarios or any eruption at all (Acocella et al., 2023). Due to the potential for eruptive activity at these volcanoes to escalate to catastrophic caldera-forming eruption scales, even non-eruptive unrest episodes can cause socio-economic issues through uncertainty around future activity and activation of precautionary mitigation efforts (e.g. Potter et al., 2015). Therefore, a detailed record of unrest periods and their potential source processes at caldera volcanoes is vital for providing a foundation on which future activity can be assessed and communicated to the public.

Taupō volcano is a large silicic caldera located within the Taupō Volcanic Zone (TVZ) rift in New Zealand's North Island (Te Ika-a-Māui) and largely obscured by

*Corresponding author: o.lamb@gns.cri.nz

Lake Taupō (Fig. 1; Barker et al., 2021). The caldera was formed by structural collapse associated with the ~25.4 ka Oruanui supereruption (Wilson, 2001; Vandergoes et al., 2013), with the spatial extent defined by a large negative (-70 mGal) gravity anomaly (Fig. 1; Davy and Caldwell, 1998; Stagpoole et al., 2020). 28 post-Oruanui eruptions have been recognised (25 during the last 12 ka) with great variation in size and eruption style, the latest and largest of which occurred at 232 ± 10 CE (Hogg et al., 2012), causing further collapse beneath the lake ('Taupō eruption'; Barker et al., 2015, 2021). This eruption was immediately followed by a sub-aqueous formation of rhyolitic lava domes that formed the Horomatangi Reefs and Waitahanui Bank (Wilson, 1993), which are sites of active hydrothermal venting (de Ronde et al., 2002) and the Lake Taupō geothermal field (Fig. 1; Bibby et al., 1995). Petrological and seismic anisotropy studies have suggested a magma reservoir is present at 5–8 km depth beneath the lake (Barker et al., 2015; Illsley-Kemp et al., 2019; Barker et al., 2021). Since 1872, 16 episodes of non-eruptive unrest have been recognised at Taupō volcano (Potter et al., 2015), the last of which took place in 2019 (Illsley-Kemp et al., 2021). Each episode was characterised by increased seismic activity within or near the caldera, often accompanied by ground deformation (Peltier et al., 2009; Potter et al., 2015; Illsley-Kemp et al., 2021; McGregor et al., 2022; Otway et al., 2022). Detailed analysis of the 2019 unrest suggested the occurrence of a magmatic intrusion into a silicic magma reservoir beneath the lake (Illsley-Kemp et al., 2021). Based on hazard, unrest, and exposure factors Taupō was ranked as Very High Threat among volcanoes in New Zealand (Miller and Jolly, 2014).

In May 2022, Taupō volcano entered a new episode of unrest with increased levels of seismic activity and ground deformation within the caldera. This episode was particularly noteworthy to the public for two reasons: 1) the Volcanic Alert Level (VAL, the system by which the activity state of a volcano is communicated to the public on a scale of 0 to 5, where ≥3 are for eruptions; Potter et al., 2014) for Taupō volcano was raised from VAL 0 (no volcanic unrest) to VAL 1 (minor volcanic unrest) for the first time in September 2022[1], and 2) a M_L 5.7 earthquake beneath the lake in November 2022 was widely felt across the North Island and generated a small (~ 0.2 m) yet complex lake tsunami (Power et al., 2023). In this article, we provide an overview of the seismic activity during this unrest episode including relocations of automatically detected earthquakes and calculated moment tensors of the largest events. Observations are interpreted in context of our current understanding of the volcanic system. Ultimately we aim to document a significant non-eruptive unrest episode to assist in recognising and interpreting future episodes at Taupō and other silicic caldera volcanoes globally.

---

[1]for historical VAL records see https://github.com/GeoNet/data/tree/main/volcanic-alert-levels, last accessed Aug. 2023

2 GeoNet Network and Methods

GeoNet is New Zealand's national monitoring programme run by GNS Science; GeoNet collects a wide range of data to monitor and respond to volcanoes, landslides, earthquakes and tsunamis (e.g. Petersen et al., 2011). The unrest episode was recorded across the GeoNet network of seismometers (GNS Science, 2021) and Global Navigation Satellite System (GNSS) stations (GNS Science, 2000) around the lake (Fig. 1). In response to the M_L 5.7 earthquake in November 2022, GeoNet installed two new broadband seismometers plus one strong-motion sensor to the east and west of the lake; data from these new stations began streaming to GeoNet on 7 and 13 December respectively. A strong-motion seismmometer was also installed on a navigation platform at Horomatangi Reefs in May 2023 but data from that sensor is not used here as it was still undergoing testing when the unrest episode ended. The Horomatangi Reefs location also hosts the only GNSS station inside the caldera (TGHO; Fig. 1), mounted on a wooden navigation structure on the reef. GeoNet routinely calculates a daily position solution from these data but a large scatter in values is observed due to birds perching on the antenna as well as the wooden construction of the site; the station was installed to capture large offsets often associated with caldera unrest.

Earthquakes during the 2022-2023 period were located by GeoNet (GNS Science, 1970), initially automatically detected, associated, and located using Seis-ComP3. Manual phase pick, location, and magnitude refinement was then undertaken within a few minutes of event occurrence by the New Zealand National Geohazards Monitoring Centre (NGMC, Te Puna Mōrearea i te Rū; Godfrey et al., 2021), which operates 24/7; automatic phase picks are only retained unmodified if they have been reviewed and confirmed to be correctly made. It is worth noting that over 50% of earthquakes beneath Lake Taupō are given a fixed depth of 5 or 10 km due to distance-to-station requirements (see cross-sections in Fig. S1). We used all GeoNet produced phase picks (automatic and manual), event associations, and event magnitudes, without further modification, and focused on relocating the earthquakes plus calculating regional moment tensors. Magnitude of completeness (M_c) and b-values were estimated using the goodness-of-fit methodology described by Wiemer and Wyss (2000). A time-series of M_c and b-values was calculated using a rolling 28-day window over the time period of analysis. Values were not estimated for windows with <10 earthquakes or a goodness-of-fit residual of <95%; these criteria excluded nearly all time windows outside the unrest period (May 2022 to May 2023) due to low earthquake detection rates.

Relocations were determined using the double-difference algorithm *tomoDD* (Zhang and Thurber, 2003), which utilises absolute phase times as well as event-pair differential times, using the double-difference method (Waldhauser and Ellsworth, 2000). We examined 1703 earthquakes for the May 2022 to May 2023 time period, from an initial 1951 events. Stations within 100 km of Lake Taupō were used for relocations
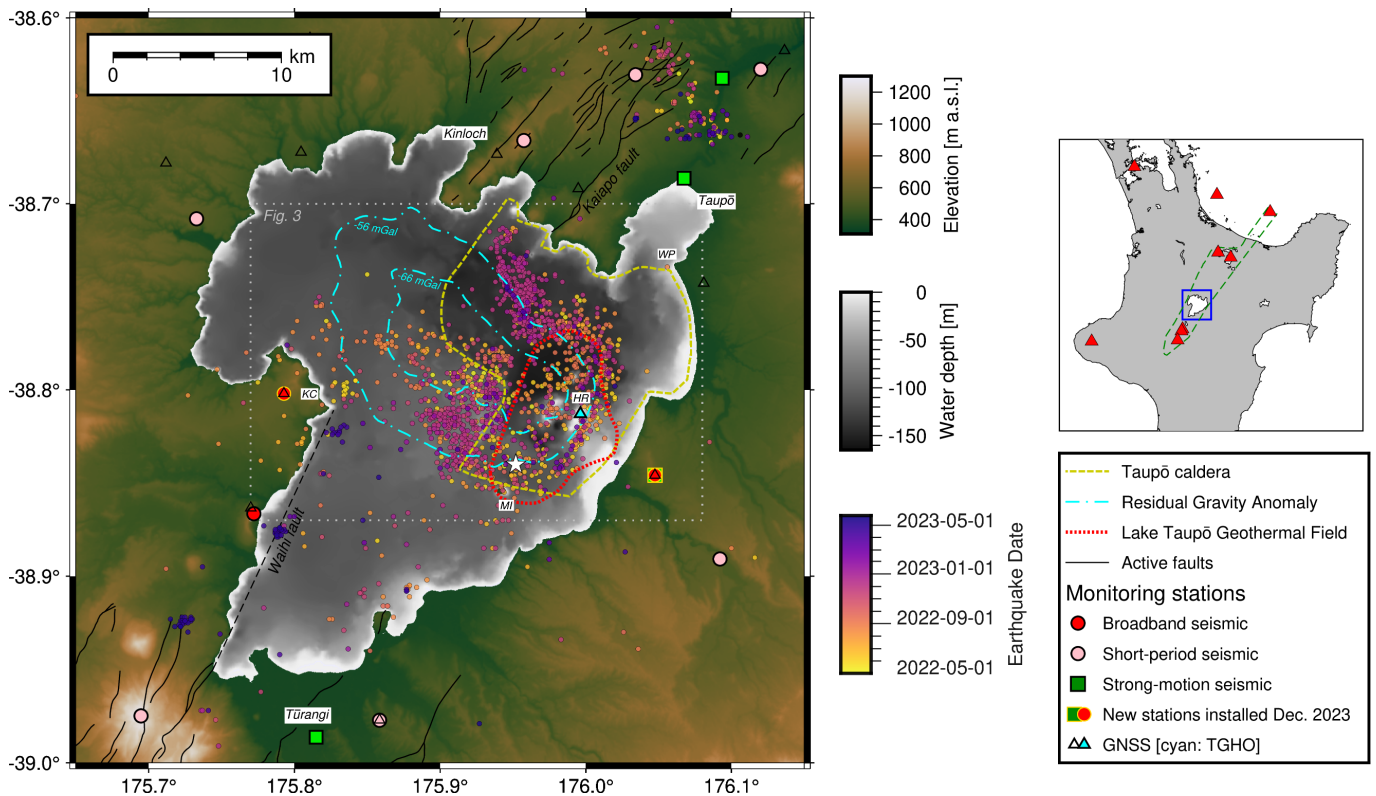
Figure 1 Overview map of Lake Taupō. Earthquakes detected and relocated during the 2022-23 unrest are shown and coloured by time. (Note that earthquakes in the northeast are related to the Wairakei and Tauhara geothermal fields and are not discussed in this paper.) The location of the 30 November M$_L$ 5.7 event is plotted as a white star. Locations of GeoNet seismic stations around the lake are shown as red triangles, pink circles, and green squares. Seismic stations with yellow outlines were added during unrest. Cyan triangle shows the TGHO GNSS station, empty triangles indicate other GNSS stations in the region but are not used in this article. Also marked are approximate outlines of the Taupō caldera (yellow dashed line; Davy and Caldwell, 1998), residual gravity anomaly contours (cyan dot-dashed line; Stagpoole et al., 2020), the Lake Taupō geothermal field (red dotted line; Bibby et al., 1995), as well as active faults (black lines; Langridge et al., 2016). KC, Karangahape Cliffs; MI, Motutaiko Island; HR, Horomatangi Reefs; WP, Wharewaka Point. Grey dotted box marks outline of area in Fig. 3. Inset shows location of Lake Taupō within the North Island of New Zealand. Also marked are locations of other active volcanoes monitored by GeoNet (red triangles) and the edges of the TVZ (green dashed line).

of earthquakes, except for events >M4 where stations further afield could be used (see Fig. S2 for map of GeoNet stations across the North Island). Events were not considered if they had observations from less than 5 stations, no S-phase picks, or an azimuthal gap greater than 310°. We note that the median azimuthal gap for relocated events was 71°, with only 7 events featuring azimuthal gap >220° (Fig. S3). Event-pair differential catalogue phase times were calculated from the absolute phase data, for all pairs of events separated by less than 9 km. Event-pair waveform-based differential times were also used, calculated using waveform cross-correlation, after application of a 2 – 12 Hz bandpass filter. In total our inversion involved 39,668 absolute P times, 7,755 absolute S times, 1,316,542 differential-phase P times, 141,570 differential-phase S times, and 372,902 waveform-based differential times. Following the approach of Zhang and Thurber (2003), higher weighting was applied to the absolute phase information during initial iteration steps, while in subsequent iteration steps the relative weighting was slowly modified, with the final iterations involving more emphasis on differential (cross-correlation-derived) phase information.

For travel-time calculation we used a 3-D velocity model developed for the southern Taupō-Tongariro region (Bannister et al., 2023, see Supplementary Material), effectively a finer-scale version of the 3D New-Zealand-scale regional model of Eberhart-Phillips et al. (2010). We note that this 3D velocity model is not optimised for the Lake Taupō region, as it was developed using seismicity north and south of the lake. In particular, sub-lake volcanic (caldera-infill) deposits, likely with low-P-wave velocity, are weakly represented by the existing 3-D velocity models; uncertainty in the 3-D velocity structure contributes to uncertainty in the absolute event depths for this unrest episode. Earthquake locations for the majority of the events in the centre of the lake may also be negatively affected by the land-based seismometer distribution; before December 2022 the closest seismometer to many of the larger-magnitude events in the centre of the lake was of the order of 15 – 20 km (Fig. 1), which is not optimal for constraining shallow event depths. Errors in the event locations were estimated, before double-difference relocation, using the vertical projection of 68% confidence ellipsoids estimated using *NLLoc* software (*NonLinLoc* from Lomax et al., 2000), where *NLLoc* determines a posterior proba-

bility density function as part of a grid search for the location solution. The median value of the minimum and maximum horizontal uncertainties for the event dataset were 1.3 km and 2.1 km respectively, while the median depth uncertainty was 2.1 km (Fig. S4). However, these errors do not reflect additional uncertainties in the absolute locations due to velocity model errors (e.g. Husen and Hardebeck, 2010).

We also applied k-means spatial clustering to aid in interpreting the spatial distribution of the relocated earthquakes; for our analysis, we employed the k-means functionality within the *scikit-learn* Python package (Pedregosa et al., 2011). The k-means algorithm groups data by attempting to assign samples to a pre-determined number of clusters of equal variance while minimizing within-cluster sum-of-squares (MacQueen, 1967). Based on the "elbow" method (Thorndike, 1953), the optimal number of clusters for earthquakes during the 2022-23 unrest was determined to be 6.

We calculated regional moment tensor (RMT) solutions (GNS Science, 2006) using the method of Herrmann (2013) for all earthquakes $M_L > 3.5$. Velocity models used to calculate theoretical Green's functions are given in Ristau (2008). The observed waveforms and Green's functions are bandpass filtered for very low frequency energy, which is less affected by Earth structure, in the range of 0.02 – 0.05 Hz. The RMT method allows for the calculation of the full seismic moment tensor, the seismic moment (M_0), and depth is determined by finding the depth with the smallest variance between the observed and synthetic waveforms. Seismic data from GeoNet stations across the North Island and northern South Island were used for the regional moment tensor solutions (see map in Fig. S7). Typically, the isotropic component of the tensor is constrained to be zero ($M_{33} = -(M_{11} + M_{22})$) and only the double-couple and CLVD components are computed; however, the isotropic component can be calculated if a large CLVD component is estimated. The isotropic component represents an explosive/implosive component and is associated with volumetric changes. A statistical F-test was carried out to ensure any RMT inversion with an isotropic component was statistically significant (e.g., Panning et al., 2001). The F-test takes the ratio of the variance of the best-fitting deviatoric solution and the full moment tensor solution $((1 - \sigma_{dev}^2)/(1 - \sigma_{full}^2))$ with the critical values of 1.14, 1.36, and 1.55 at the 75%, 95%, and 99% confidence levels respectively.

3 Unrest chronology

GeoNet detected increased seismic activity beneath Lake Taupō in May 2022, ending a period of relative quiescence (median of 1 earthquake per week) following the 2019 unrest (Fig. 2a, b). Over the next 13 months, >1780 earthquakes were detected beneath the lake (median of 23 events per week), with a b-value and M_c of 1.0 and 1.6, respectively (Fig. 2d). All of the earthquakes were identified as volcano-tectonic, with no low-frequency events or tremor observed. We identified four separate activity phases during the 2022-23 unrest based on weekly earthquake detection rates.

Phase A lasted from 1 May through to Mid-September 2022 with over 650 earthquakes detected beneath the lake. Earthquakes were detected at 10–50 events per week, with no clear acceleration or trends over time. The largest number of earthquakes occurred near the end of the phase, with 86 events over 1 week. Most of the events within this week were aftershocks to the largest magnitude event during this phase, a M_L 4.2 on 9 September that was widely felt around the lake (Fig. 2c). By comparison, phase B of the unrest from mid-September to 29 November was relatively quiet but still higher than pre-unrest activity. 10 – 25 events of $M_L < 3$ were detected per week with only three earthquakes at M_L 3.1 – 3.5. B-value and M_c values fluctuated throughout both phases, with peaks in b-values of 1.3 and 1.7 in early May and early July, respectively (Fig. 2c). GNSS measurements since late May at TGHO indicated a <50 mm total uplift up to the end of November (Fig. 2a). The VAL for Taupō was raised from 0 to 1 on 20 September due to the continuing seismic unrest and ground deformation suggesting a magmatic process instead of rift-related tectonic activity.

Phase C from 30 November to 31 December includes the most intense period of seismic activity during the unrest episode. The largest magnitude earthquake for the whole unrest episode occurred at 10:47 UTC on 30 November with an estimated M_L 5.7. This event generated strong shaking (Fig. S6b; GNS Science, 2023), with a maximum vertical Peak Ground Acceleration of just under 100 cm.s^{-2} recorded at site WAIS (28 km distant; GNS Science, 2020) and over 5400 felt reports from across the North Island were reported on the GeoNet website (Fig. S6a; GNS Science, 2015). Multiple landslides were triggered around the lake, with a small tsunami also recorded within the lake, the first of its kind instrumentally recorded at Taupō. The tsunami was partly triggered by a landslide at Wharewaka Point, located on the southern margin of the Taupō township (WP in Fig. 1) as well as uplift on the lake floor from the earthquake (Power et al., 2023). GNSS measurements at Horomatangi Reefs measured a >200 mm upward motion during and immediately after the earthquake (Fig. 2a). The mainshock was preceded by a M_L 3.9 foreshock at 05:37 UTC, and followed by 3 M_L 4.2–4.5 aftershocks within the next 15 hours. 581 earthquakes were detected beneath the lake over the following week, with 778 in total before the end of December. Seismic b-values immediately following the mainshock dropped to 0.7 before recovering to 0.9 for most of phase C, which finished with a sharp rise to 1.3 at the end of December 2022 (Fig. 2c). The earthquake rate for the aftershock sequence following the M_L 5.7 on 30 November did not follow the Omori-Utsu law that is characteristic of tectonic earthquakes and their aftershocks (Fig. 2e; Utsu et al., 1995).

Phase D concluded the unrest episode and was defined by a lower rate of weekly earthquakes, with 184 detections from 1 January to 30 May 2023. Fewer than 10 events were detected per week, except for two minor swarms in early March 2023 and late April 2023, with peaks rates of 30 – 36 earthquakes per week. The March swarm coincided with the largest magnitude event dur-
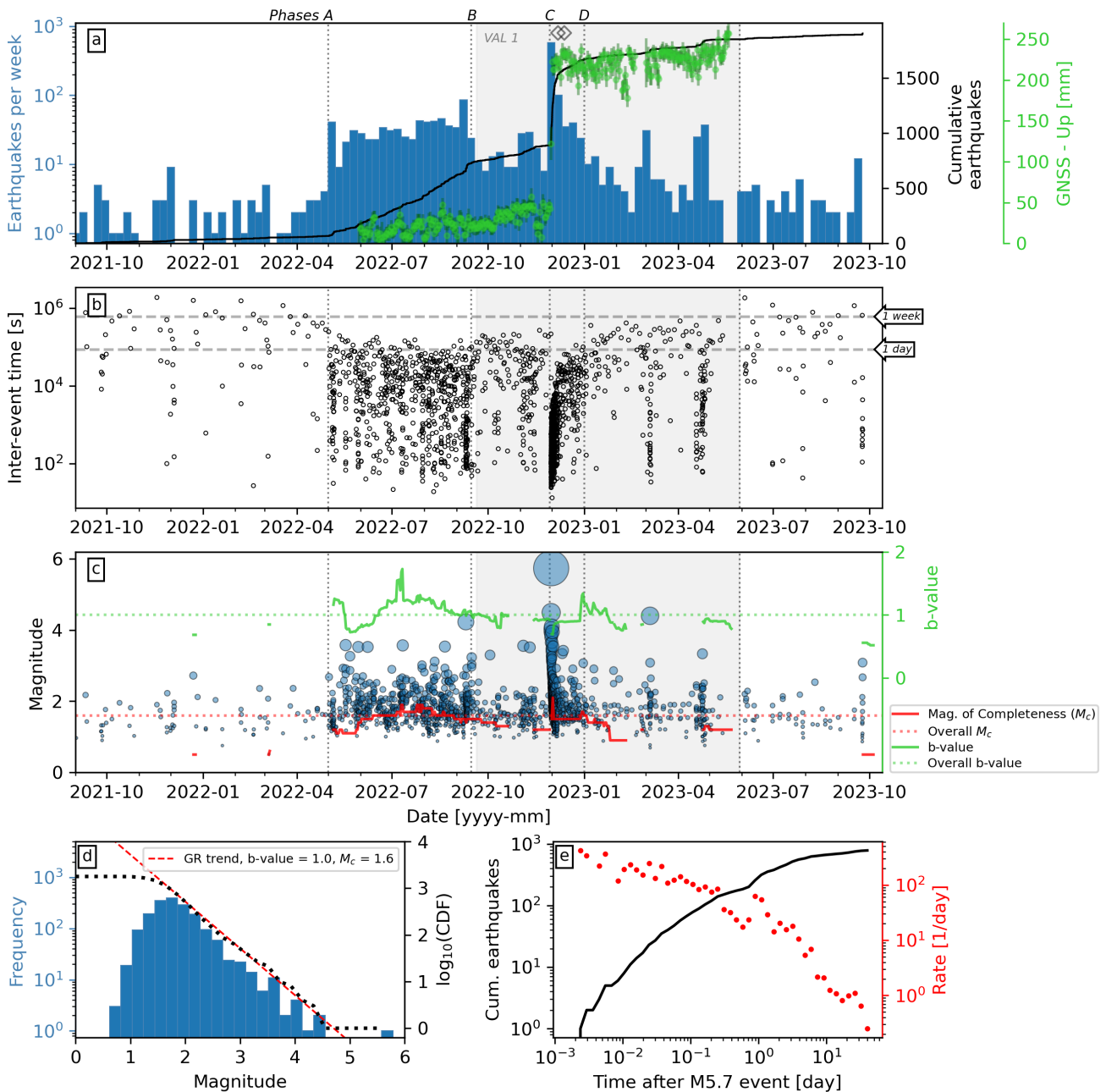
Figure 2 (a) Number of earthquakes detected beneath Lake Taupō per week. Black line indicates cumulative number of events. Green circles indicate upward component of TGHO GNSS station located on Horomatangi Reefs. Diamonds indicate dates when new seismic stations were added to network around the lake. Letters above panel indicate the start times of different phases of the unrest, as described in main text. (b) Inter-event times in seconds between earthquakes. (c) Earthquake magnitudes over time. Each point is sized by their magnitude. Also plotted are rolling b-values (green line) and magnitude of completeness (red line) for previous 28 day period. Values were not estimated for periods with <10 earthquakes. Red and green dotted lines indicate overall magnitude of completeness and b-value values, respectively, as indicated in panel d. Grey shading in panels a-c indicates time period the VAL was set to 1. (d) Magnitude-frequency distribution for all events in panels a-c, including the cumulative distribution function (dotted line) and Gutenberg-Richter trend (GR trend, red dashed line). (e) Earthquake rate decay for earthquakes for 60 day period after M_L 5.7 event on 30 November. Plotted are cumulative number of earthquakes (black line) and occurrence rate of earthquakes (red dots).

ing this phase, a M_L 4.4 on 5 March. B-values dropped from 1.3 to 0.7 in January to February 2023 before a period where no values were estimated due to low numbers of events or low goodness-of-fit residuals (Fig. 2c). However, b-values of approximately 0.9 were estimated following the late April swarm. Phase D, and the 2022-23

unrest episode, concluded in late May 2023 with a return to background activity levels. This was characterised by earthquake inter-event times greater than 1 week (Fig. 2b) and a cessation in ground deformation (Fig. 2a). As a result, the VAL for Taupō was lowered to 0 on 30 May 2023 after 252 days at VAL 1. From the end of May un-

til the time of submission, earthquake detection rates beneath the lake remained low at rates similar to background activity prior to the 2022-23 unrest.

4 Earthquake location and source parameters

The majority of earthquakes were distributed within the Taupō caldera (Fig. 1). Each phase of the 2022-23 unrest episode at Taupō shows a distinct distribution of locations beneath the lake (Fig. 3, 4, S5). Compared to the initial locations determined by GeoNet, the relocated earthquakes are more concentrated in distinct clusters beneath the lake (Fig. S1, S5).

In phase A from 1 May to 14 September, most of the earthquakes form a somewhat elliptical ring centred on Horomatangi Reefs, aligned NE-SW, of approximately 8 – 13 km and 5 – 8 km maximum and minimum dimensions, respectively (Fig. 3a). Some of the early earthquakes during this phase were located in a small group near Karangahape Cliffs on the western side of the lake. This group included a M_L 3.5 on 29 May with a double-couple normal-fault moment tensor solution with a NE-SW (rift parallel) fault plane. A M_L 3.5 on 20 August was located on the southern end of the elliptical group and also showed a normal-fault moment tensor. The M_L 4.2 on 9 September was located 2 km north of Horomatangi Reefs and showed a double-couple moment tensor, with a vertical fault plane oriented NW-SE. Most of the earthquakes during phases A and B were associated with k-means spatial clusters 3 and 5 (Fig. 4).

Most of the earthquakes of phase B are found in two groups, located at the north and south ends of the ellipse grouping seen in phase A (Fig. 3b); the southern group is located directly beneath Motutaiko Island. Two moment tensors were estimated for earthquakes of M_L 3.5 and 3.6 on 3 and 9 November, respectively. Each moment tensor has a double-couple normal-fault signature event oriented NE-SW (rift parallel).

Phase C earthquakes immediately preceding and following the M_L 5.7 on 30 November are mostly located within two distinct groups beneath Lake Taupō (Fig. 3c). The mainshock was located approximately 2 km NNE of Motutaiko Island at 9.3 km depth. The M_L 3.9–4.5 foreshock and aftershock events were located northeast and north-west of the mainshock, respectively. One group of earthquakes was located NW of the mainshock, with events aligned along two perpendicular linear features, oriented approximately NE-SW and E-W; most events within this group were divided between clusters 3 and 6 (Fig. 4). The second group was located approximately 5 km north of the first, forming a linear feature oriented NNW-SSE and roughly aligned with the -56 mGal residual gravity anomaly contour (Fig. 3c). The northern end of the group aligns with a small number of earthquakes seen in phase A (Fig. 3a). Almost all of the earthquakes in this northern group were allocated to cluster 1 (Fig. 4). A smaller group of earthquakes was located to the east of Horomatangi Reefs, and includes the M_L 3.9 foreshock to the M_L 5.7 mainshock. Moment tensor inversions for earthquakes during this phase show a variety of solutions, most show-

ing double couple normal-fault solutions on rift-aligned planes. Two events within the southern cluster show NW-SE fault orientations, while two events in the northern cluster show inclined strike-slip faulting. The deviatoric moment tensor solution for the M_L 5.7 event has a best fit at 3 km depth with a large CLVD component of 66% (Fig. S7). The full moment tensor solution for the M_L 5.7 event is deeper (7 km; Fig. 3C, S8) with a large isotropic component (38%); the deviatoric part is 62%, of which 56% is pure double-couple and 6% is CLVD. The best-fitting deviatoric solution has σ^2_{dev} = 0.734 and full solution σ^2_{full} = 0.806 which gives an F-value of 1.37, above the 95% confidence threshold. The M_L 5.7 earthquake was the only event in the whole unrest sequence to feature a non-negligible isotropic component.

Earthquakes during phase D were focused in the same areas where significant seismic activity was observed during phase C (Fig. 3d). The moment tensor solution for the M_L 4.4 on 5 March showed a double-couple normal fault event oriented NW-SE. There was also a small group of events located under the western side of the lake, 2 km directly south of the small group seen in phase A in the same area and associated with cluster 3 (Fig. 4).

5 Discussion

5.1 Seismic characteristics of 2022-23 unrest

We recognised four phases of activity within a 13 month period of unrest, each distinguished by differing earthquake occurrence rates, magnitudes, and locations (Figs. 2, 3). Earthquake locations mostly coincide with a significant overlap of the Taupō caldera and residual gravity anomaly associated with the Oruanui caldera (Fig. 1; Davy and Caldwell, 1998; Wilson, 2001; Stagpoole et al., 2020) as well as a geothermal field and active hydrothermal venting (Bibby et al., 1995; de Ronde et al., 2002). Most of the moment tensor estimates in this area feature double-couple normal-fault solutions on rift-aligned planes, with a few showing NW-SE alignment instead (Fig. 3); the main exception is the non-double couple reverse faulting moment tensor solution for the M_L 5.7 event which is discussed in more detail below. Altogether, this central main group of earthquakes may represent the reactivation of faults associated with the Oruanui and Taupō caldera structures. Normal and strike-slip faulting with NW-SE T-axes are typical due to extensional rifting in the Taupō Volcanic Zone (Hurst et al., 2002). The faulting mechanisms could also interpreted as normal motion along sub-vertical faults due to uplift of the footwall. As there is no way of identifying which nodal plane is the actual fault plane, then both processes could have occurred during the 2022-23 unrest at Taupō volcano.

A significant linear NNW-SSE cluster of earthquakes also occurred during phase C (cluster 1; Figs. 3c,4). This cluster does not follow the general NE-SW trend of rifting faults, but two moment tensors within this area include strike-slip fault plane solutions that may align along this trend. Furthermore, this cluster is aligned along residual gravity anomaly contours that delineate
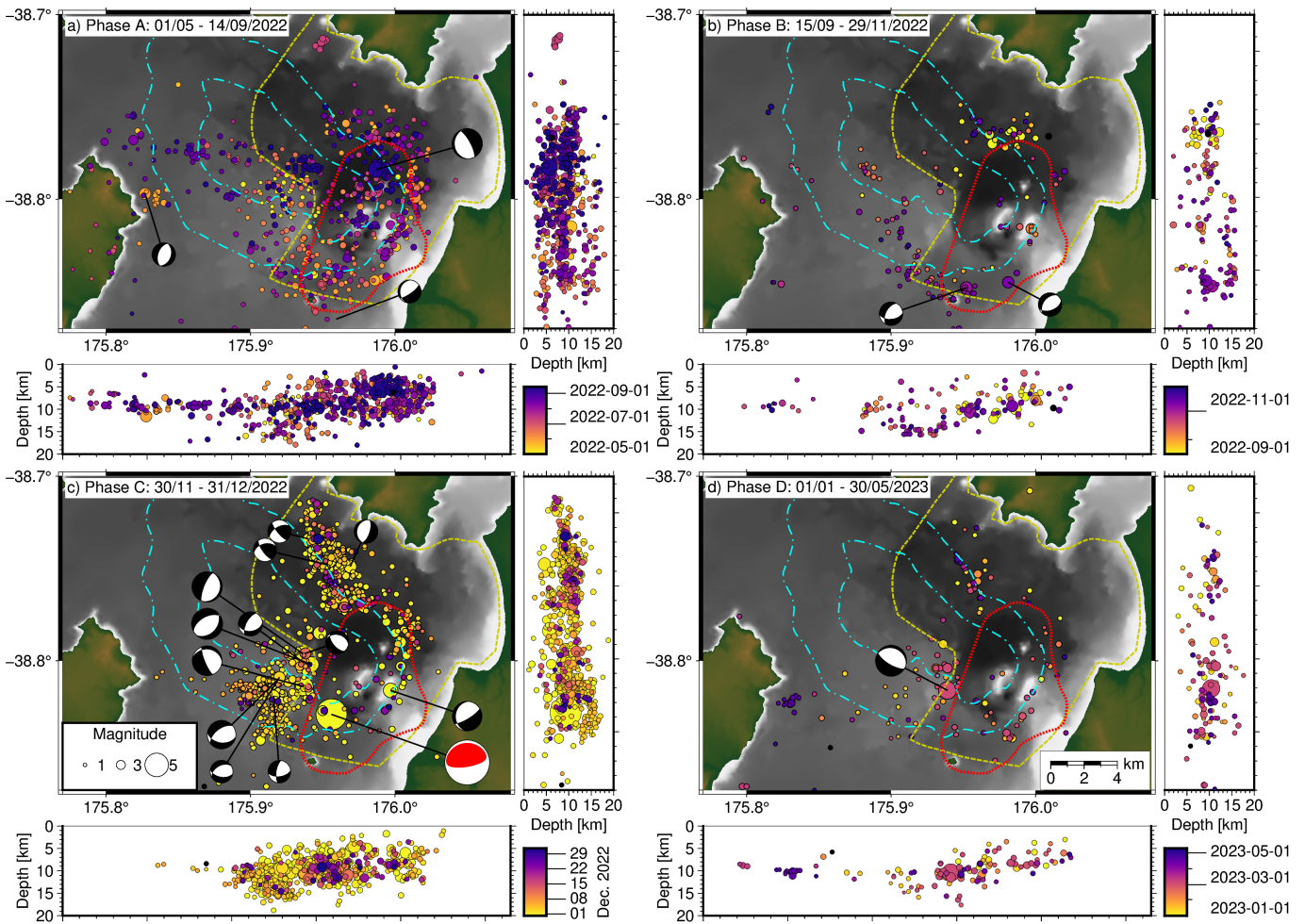
Figure 3 Progression of earthquake locations and depths during the unrest. Each panel details relocated earthquakes with each phase of the unrest period, coloured by time (colorbar at bottom right of figure). Moment tensors for earthquakes >M3.5 are also plotted on lower hemisphere projections; the red moment tensor for the M_L 5.7 highlights the non-double couple nature of the solution. Sub-panels below and right of each map are longitudinal and latitudinal cross-sections, respectively. Yellow dashed line outlines the Taupō calderas, cyan dot-dashed lines indicate residual gravity anomalies associated with the Oruanui eruption caldera, and red dotted lines indicate the Lake Taupō geothermal field.

caldera boundaries formed during the Oruanui eruption (Davy and Caldwell, 1998; Stagpoole et al., 2020). It is worth noting that the northern end is aligned with a small group in the same area during phase A (Fig. 3a) and may intersect with a sub-aqueous section of the Kaiapo Fault (Fig. 1). We do not see clear temporal movement of earthquakes in any direction within this cluster that may indicate, for example, the migration of fluids. Therefore, this cluster likely represents reactivation of one or more faults associated with at least one of the major caldera collapse events in the past. Two smaller groups of earthquakes were also observed beneath the western margin of the lake near Karangahape Cliffs during phases A and D (Fig. 3a, d), including a double-couple normal-faulting rift-aligned moment tensor estimated in this area during phase A. This area represents the northern-most end of the Waihī Fault, as well as the north-western edge of the main seismic activity seen during the 2019 unrest (Illsley-Kemp et al., 2021; Illsley-Kemp et al., 2022). These clusters likely represent brief reactivations of faults in area where tectonic and caldera faults intersect.

The 30 November M_L 5.7 event represents the largest

event recorded beneath the lake in historical times. Previous M_L>5 events beneath or near the lake were recorded in the 2019 unrest episode (Illsley-Kemp et al., 2021), and in 1984, 1982, 1968, 1956, 1952, and 1922 (Potter et al., 2015). The full moment tensor solution for the M_L 5.7 event showed a non-negligible non-double-couple with a large isotropic component (Fig. S8). The improvement in the waveform fits for the full solution (Fig. S8) compared with the deviatoric solution (Fig. S7) at the 95% confidence level is evidence for a source with a double-couple reverse faulting mechanism with a shallow dipping NNW plane and steeply dipping SSE plane, and a non-negligible isotropic explosive/inflation component. Simultaneously the TGHO GNSS station recorded a 180 mm vertical and >250 mm south-eastern lateral movement (Figs. 2a, S9). Altogether, the earthquake and ground deformation may be interpreted as the opening of a sub-horizontal tensile crack together with reverse motion along a sub-vertical fault. However, a normal fault with a shallow dipping SSE plane and steeply dipping NNW plane is also consistent with the data. While there is evidence for a isotropic component to the source, we cannot rule out a source with a
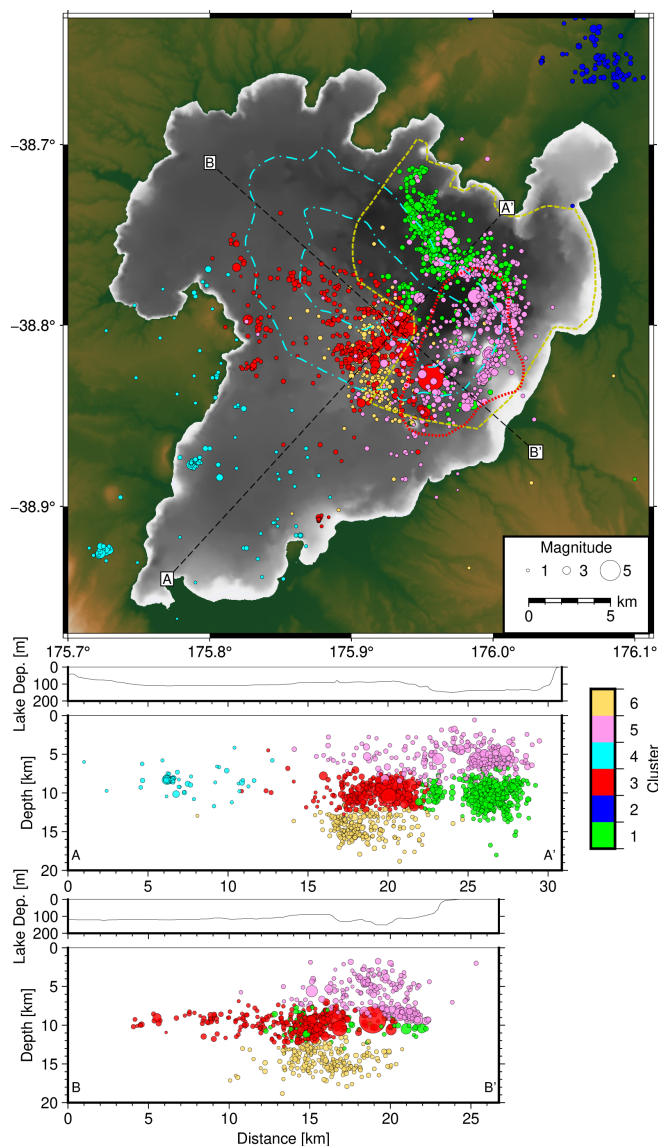
Figure 4 Map and cross-sections of relocated earthquakes during the unrest, coloured by k-means spatial clustering. Yellow dashed line outlines the Taupō calderas, cyan dot-dashed lines indicate residual gravity anomalies associated with the Oruanui eruption caldera, and red dotted lines indicate the Lake Taupō geothermal field. Cross-sections show earthquakes located within 4 km horizontal distance of lines in main panel. Above each cross-section is the bathymetry of the lake floor. (See Fig. S12 for a 3D version of the plot.)

large CLVD component and no isotropic component.

The moment tensor and the tsunamigenic nature of the M_L 5.7 event resembles earthquakes detected at submarine volcanoes in the Izu-Bonin and Kermadec arcs for which a 'trapdoor' faulting mechanism has been modelled (Sandanbata et al., 2022, 2023). This faulting mechanism has also been observed at the subaerial Sierra Negra volcano, Galápagos Islands (e.g., Amelung et al., 2000; Jónsson, 2009; Gregg et al., 2022). We also observed two distinct clusters of earthquakes after the M_L 5.7 earthquake (Fig. 3c). In 2018, stress changes due to trapdoor faulting at Sierra Negra may have induced tensile failure on the opposite side of the caldera (Gregg et al., 2022); it's possible that a similar process occurred

in Taupō to generate these distinct clusters. Finally, it is worth noting that the estimated depth of the mainshock (7 – 9.3 km) places it near or below the proposed depths of the magma reservoir beneath Taupō (5 – 8 km; Barker et al., 2015). Further work with joint seismic-geodetic inversion using a ring fault-crack composite system is needed to refine the source process and effects of the M_L 5.7 earthquake.

5.2 Drivers of 2022-23 unrest

Seismic activity within silicic caldera volcanoes such as Taupō has been attributed to magmatic intrusion (e.g. Saunders, 2001; Newman et al., 2001; Benson et al., 2021; Illsley-Kemp et al., 2021) and/or migration of hydrothermal fluids along structural features such as faults (e.g. Waite and Smith, 2002; Bannister et al., 2016; Miller et al., 2017; Hotovec-Ellis et al., 2018; Zhan et al., 2019). Lake Taupō lies within the TVZ rift therefore seismic unrest may also be related to fault-slip during tectonic rifting activity. 90% of earthquakes within the TVZ occur at <10 – 15 km depths which may approximate the brittle-ductile boundary within this area of high heat flow (Ellis et al., 2021). Most of the earthquakes during 2022-23 unrest were located shallower than 15 km (Figs. 3, 4) and similar depth ranges were observed for earthquakes during the 2019 unrest (Illsley-Kemp et al., 2021). However, most earthquake clusters and moment tensors during the 2022-23 unrest were not aligned with the NE-SW rift-faulting trend in the region (Fig. 3; Langridge et al., 2016). Furthermore, rift-related earthquake sequences in the TVZ are generally relatively short-lived (days to weeks) and are confined to a relatively small epicentral area (a few square km; Sherburn, 1992; Hurst et al., 2008). We also observe that the aftershock sequence does not conform to the Omori-Utsu earthquake-rate-decay law (Fig. 2e; Utsu et al., 1995) which suggests a non-tectonic origin; a similar observation was made following a M 5.3 earthquake during the 2019 unrest episode (Illsley-Kemp et al., 2021). Lastly, vertical GNSS measurements at Horomatangi Reefs (TGHO; Fig. 1), a station located within the Taupō caldera, show a coincidental contemporaneous uplift during the unrest period (Fig. 2a). Therefore, we propose the majority of earthquakes during the 2022-23 unrest were not likely due to rift-related faulting.

The movement of hydrothermal fluids within calderas may be characterised by clear delineations along fault structures, a directional migration of earthquake hypocentres over time, and the detection of low-frequency earthquakes (i.e. long-period events or tremor; Waite and Smith, 2002; Bannister et al., 2016; Hotovec-Ellis et al., 2018). Linear features within groups of located earthquakes during the 2022-23 unrest (Figs. 3, 4) could be due to reactivation of faults due to hydrothermal fluids. At Taupō, we did not observe any clear migration of earthquake locations within clusters over time nor were any low-frequency earthquakes (i.e. long-period or tremor) detected over the period of unrest. However, the latter observation may have been precluded by a lack of broadband seismometers within 10 – 15 km of the majority of seismic activity during the

unrest (Fig. 1). Therefore, while we do not see strong evidence for hydrothermal fluid movements causing the seismic activity during the unrest, we cannot rule out this process due to limitations in the monitoring network.

A notable feature of the seismic activity during the 2022-23 unrest is that most of the earthquakes were located in a region that coincided with Taupō caldera structures (Figs. 1, 3, 4; Davy and Caldwell, 1998), a large residual gravity anomaly defining the Oruanui eruption caldera (Stagpoole et al., 2020), and the Lake Taupō geothermal field (Bibby et al., 1995). This region is considered the most likely location of recent magmatic activity (Barker et al., 2021) which is manifested by active hydrothermal venting near Horomatangi Reefs (de Ronde et al., 2002). We observed variations in b-values throughout the period of unrest, with a peak of 1.7 in July 2022 during phase A (Fig. 2c). Increases in b-values due to increased pore pressure and/or crustal heterogeneity around magmatic intrusions have been observed in Japan and USA (Wyss et al., 1997; Wiemer et al., 1998). Together with the uplift observed at TGHO during the unrest (Fig. 2a), we therefore suggest the seismic activity during the 2022-23 unrest period was caused by the reactivation of faults triggered by inflation of a magmatic body beneath Horomatangi Reefs starting in May 2022. This mechanism is similar to what was proposed as the cause of the 2019 unrest at Taupō (Illsley-Kemp et al., 2021).

5.3 Comparison with previous unrest

With >1780 earthquakes detected, the 2022-23 unrest episode had more earthquakes than detected during the 2019 (906 earthquakes) and 2008-10 (920) unrest episodes at Taupō volcano (Fig. S10). Furthermore, the 2022-23 episode included the largest magnitude earthquake detected beneath the lake in historical times and the first lake tsunami or large wave since 1956 (Potter et al., 2015). There is a strong overlap in earthquake locations during the 2022-23 and 2008-10 episodes (Fig. S10a). There was also a small group of earthquakes in August 2008 that coincides with the northern margin of cluster 1 in phase C (Fig. 3c, 4). However, we should note differences in seismometer network configuration and location methodologies (including velocity models employed) between the two time periods adds uncertainty to the overlap. Nevertheless, it may be reasonable to conclude that the 2022-23 unrest reactivated faults observed during the 2008-09 episode. In contrast, most of the 2022-23 earthquakes were located within a previously 'aseismic' region observed north of the main cluster of earthquakes in the 2019 unrest episode (Fig. S10b; Illsley-Kemp et al., 2021). This region was previously used to define a hypothetical 80 – 250 km^2 area for the Taupō magmatic system with brittle-ductile transition zones on the margins; the large areal extent was due to a lack of seismicity defining the western margin in 2019. In light of the 2022-23 earthquake locations (Fig. 1,3,4), it may be reasonable to conclude that the magmatic system cannot be constrained by the 'aseismic' zone observed in 2019. Alternatively, we propose that

different faults beneath the lake were reactivated during the 2019 and 2022-23 unrest episodes due to magmatic intrusions of differing locations, dimensions, depths, and/or orientations. As mentioned previously, further work with geodetic modelling is required to help constrain the static stress fields from various magmatic intrusion scenarios within Taupō volcano.

5.4 Monitoring challenges

Each recent unrest episode at Taupō volcano has highlighted the challenges of monitoring a large caldera beneath a lake. The water restricts locating seismic and geodetic instrumentation directly above earthquake activity, and results in larger errors in seismic depth estimations. Two new seismic stations were installed on the east and west margins of the lake shortly after the M_L 5.7 earthquake on 30 November. We investigated the effect of adding two new stations on routine earthquake detection and locations within Lake Taupō. The full routine earthquake location algorithm was run using the original network in parallel with the updated network for a period of 3 months. There was no significant change in horizontal location errors, but a greater proportion of earthquakes (54 versus 34%) were able to have a calculated depth estimate instead of a fixed depth (due to distance-to-station requirements); there was no significant change in the total number of earthquake detections observed. A new strong-motion sensor installed in early May 2023 at the Horomatangi Reefs site is intended to improve depth resolution for earthquakes beneath the lake but, due to large background noise levels, it is expected to only be effective for earthquakes of $M_L > 3$.

One of the key decisions a volcano observatory makes when setting alert levels for volcanoes is understanding when activity levels have returned to 'background'. This is particularly challenging for a volcano obscured by a lake within a tectonic rift zone. It may not be immediately clear when seismic activity is related to volcanism or rifting, particularly outside of the inferred caldera boundaries. One of the key parameters used to assess the level of seismic activity within the lake during the 2022-23 unrest episode was the inter-event time (i.e. repose interval) between earthquakes (Figs. 2b, S11). We looked at the distribution of inter-event times for earthquakes within the northern half of the lake (Fig. S11a) during background periods (2013-18 and 2020-21) and two unrest periods (2019 and 2022-23). The higher rate of earthquakes during unrest episodes creates a significant difference between the distributions of background and unrest inter-event times (Fig. S11b). We found that distribution of inter-event times for earthquakes during unrest episodes is almost exclusively contained below the 75th percentile of background inter-event times (approximately 9.3 days during 2013-18; Fig. S11b). In other words, we estimated that 25% of inter-event times during 'background' activity would be 9.3 days or more. A two week repose in earthquake activity was observed in late May 2023 (Fig. S11d) while at the same time the daily GNSS timeseries around Lake Taupō indicated a cessation in ground de-

formation. With both seismic and geodetic measurements indicating a return to background levels the VAL was set at 0 (i.e. no volcanic unrest) on 30 May, thus ending the 2022-23 unrest episode.

6 Conclusions

Taupō volcano underwent a period of heightened unrest from May 2022 to May 2023 which was more intense than previous instrumented unrest episodes in terms of earthquake rates and magnitudes. Over 1700 earthquakes were detected during this period, including a M_L 5.7 on 30 November that was notable for generating a small tsunami within the lake. Four separate activity phases were identified based on differing earthquake detection rates. Most of the earthquakes were relocated to within an area with significant overlap of caldera structures and geothermal features. Regional moment tensor solutions for the largest events were dominated by double-couple mechanisms, except for the M_L 5.7 event which featured a non-negligible non-double-couple and isotropic components. Our observations suggest the earthquakes were due to reactivation of faults beneath the lake due to a possible magma intrusion at depth. This unrest episode highlighted the challenges in monitoring Taupō volcano due to the presence of the lake which restricts instrumentation options. Analysing earthquake inter-event distributions could be a helpful tool in defining future unrest occurrence. Ultimately, the 2022-23 unrest episode has provided new insights into how seismic unrest evolves at Taupō which will improve our understanding of future events at Taupō and other silicic calderas.

Acknowledgements

Data and code availability

GeoNet continuous seismic data (GNS Science, 2021), automatic locations (GNS Science, 1970), moment tensor solutions (GNS Science, 2006), and GNSS data (GNS Science, 2000) are openly available through the GeoNet website (www.geonet.org.nz, last accessed Aug. 2023). The 3D velocity model used for travel-time calculations is available as a supplementary file, along with the moment tensors plotted in this article. This paper benefited from various Python packages including ObsPy (Krischer et al., 2015), ObsPlus (Chambers et al., 2021), Matplotlib (Hunter, 2007), scikit-learn (Pedregosa et al., 2011), and PyGMT (Uieda et al., 2023).

Competing interests

The authors have no competing interests.

References

Acocella, V., Ripepe, M., Rivalta, E., Peltier, A., Galetto, F., and Joseph, E. Towards scientific forecasting of magmatic eruptions. *Nature Reviews Earth & Environment*, 2023. doi: 10.1038/s43017-023-00492-z.

Amelung, F., Jónsson, S., Zebker, H., and Segall, P. Widespread uplift and 'trapdoor' faulting on Galápagos volcanoes observed with radar interferometry. *Nature*, 407(6807):993–996, 2000. doi: 10.1038/35039604.

Bannister, S., Sherburn, S., and Bourguignon, S. Earthquake swarm activity highlights crustal faulting associated with the Waimangu–Rotomahana–Mt Tarawera geothermal field, Taupo Volcanic Zone. *Journal of Volcanology and Geothermal Research*, 314:49–56, 2016. doi: 10.1016/j.jvolgeores.2015.07.024.

Bannister, S., Johnson, J., Guo, H., Bennington, N., Heise, W., and Zhang, H. Seismic imaging of the mid-crustal magmatic system beneath Ruapehu and Tongariro stratovolcanoes, Taupo Volcanic Zone. In *http://www.iavceivolcano.org/content/uploads/2021/03/iavcei-2023-book-of-abstracts.pdf*. IAVCEI 2023 Scientific Assembly, 2023.

Barker, S. J., Wilson, C. J. N., Allan, A. S. R., and Schipper, C. I. Fine-scale temporal recovery, reconstruction and evolution of a post-supereruption magmatic system. *Contributions to Mineralogy and Petrology*, 170(1):5, 2015. doi: 10.1007/s00410-015-1155-2.

Barker, S. J., Wilson, C. J., Illsley-Kemp, F., Leonard, G. S., Mestel, E. R., Mauriohooho, K., and Charlier, B. L. Taupō: an overview of New Zealand's youngest supervolcano. *New Zealand Journal of Geology and Geophysics*, 64(2–3):320–346, 2021. doi: 10.1080/00288306.2020.1792515.

Benson, T. W., Illsley-Kemp, F., Elms, H. C., Hamling, I. J., Savage, M. K., Wilson, C. J. N., Mestel, E. R. H., and Barker, S. J. Earthquake Analysis Suggests Dyke Intrusion in 2019 Near Tarawera Volcano, New Zealand. *Frontiers in Earth Science*, 8:606992, 2021. doi: 10.3389/feart.2020.606992.

Bibby, H., Caldwell, T., Davey, F., and Webb, T. Geophysical evidence on the structure of the Taupo Volcanic Zone and its hydrothermal circulation. *Journal of Volcanology and Geothermal Research*, 68(1–3):29–58, 1995. doi: 10.1016/0377-0273(95)00007-H.

Chambers, D. J., Boltz, M., and Chamberlain, C. ObsPlus: A Pandas-centric ObsPy expansion pack. *Journal of Open Source Software*, 6(60):2696, 2021. doi: 10.21105/joss.02696.

Davy, B. and Caldwell, T. Gravity, magnetic and seismic surveys of the caldera complex, Lake Taupo, North Island, New Zealand. *Journal of Volcanology and Geothermal Research*, 81 (1–2):69–89, 1998. doi: 10.1016/S0377-0273(97)00074-7.

de Ronde, C., Stoffers, P., Garbe-Schönberg, D., Christenson, B., Jones, B., Manconi, R., Browne, P., Hissmann, K., Botz, R., Davy,

B., Schmitt, M., and Battershill, C. Discovery of active hydrothermal venting in Lake Taupo, New Zealand. *Journal of Volcanology and Geothermal Research*, 115(3–4):257–275, 2002. doi: 10.1016/S0377-0273(01)00332-8.

Eberhart-Phillips, D., Reyners, M., Bannister, S., Chadwick, M., and Ellis, S. Establishing a versatile 3-D seismic velocity model for New Zealand. *Seismological Research Letters*, 81(6):992–1000, 2010. doi: 10.1785/gssrl.81.6.992.

Ellis, S. M., Bannister, S., Van Dissen, R. J., Eberhart-Phillips, D., Holden, C., Boulton, C., Reyners, M. E., Funnell, R. H., Mortimer, N., and Upton, P. New Zealand Fault-Rupture Depth Model v1.0: a provisional estimate of the maximum depth of seismic rupture on New Zealand's active faults. *GNS Science Report*, 2021/08:47, 2021. doi: 10.21420/4Q75-HZ73.

GNS Science. GeoNet Aotearoa New Zealand Earthquake Catalogue. 1970. doi: 10.21420/0S8P-TZ38.

GNS Science. GeoNet Aotearoa New Zealand Continuous GNSS Network - Time Series Dataset. 2000. doi: 10.21420/30F4-1A55.

GNS Science. GeoNet Aotearoa New Zealand Earthquake Moment Tensor Solutions. 2006. doi: 10.21420/MMJ9-CZ67.

GNS Science. GeoNet Aotearoa New Zealand Felt Rapid Dataset. 2015. doi: 10.21420/RS7F-VE53.

GNS Science. GeoNet Aotearoa New Zealand Strong Motion Data Products. 2020. doi: 10.21420/X0MD-MV58.

GNS Science. GeoNet Aotearoa New Zealand Seismic Digital Waveform Dataset. 2021. doi: 10.21420/G19Y-9D40.

GNS Science. GeoNet Aotearoa New Zealand Shaking Layers Dataset. 2023. doi: 10.21420/J856-2J84.

Godfrey, H. J., Crighton, M., Wright, K. R., Banks, M. P., Fromont, A., Gomez, A., Helliwell, M., James, L. M., Legenkyy, A., McClintock, J. D. B., O'Hagan, S., Presow, K. M., Pritchard-Thorsen, R., Rapley, C. M. J., Siemer, K., Tate, R., Thomas-Long, A., Tuckett, F. F., Watson, E., Watson, T., Wood, M. J., Wylie-Cheer, B., and Zirk, C. The National Geohazards Monitoring Centre Te Puna Mōrearea i te Rū, GNS Science, New Zealand, 2021. doi: 10.1190/segam2021-3583086.1.

Gregg, P. M., Zhan, Y., Amelung, F., Geist, D., Mothes, P., Koric, S., and Yunjun, Z. Forecasting mechanical failure and the 26 June 2018 eruption of Sierra Negra Volcano, Galápagos, Ecuador. *Science Advances*, 8(22):eabm4261, 2022. doi: 10.1126/sciadv.abm4261.

Herrmann, R. B. Computer Programs in Seismology: An Evolving Tool for Instruction and Research. *Seismological Research Letters*, 84(6):1081–1088, 2013. doi: 10.1785/0220110096.

Hogg, A., Lowe, D. J., Palmer, J., Boswijk, G., and Ramsey, C. B. Revised calendar date for the Taupo eruption derived by ^{14}C wiggle-matching using a New Zealand kauri ^{14}C calibration data set. *The Holocene*, 22(4):439–449, 2012. doi: 10.1177/0959683611425551.

Hotovec-Ellis, A. J., Shelly, D. R., Hill, D. P., Pitt, A. M., Dawson, P. B., and Chouet, B. A. Deep fluid pathways beneath Mammoth Mountain, California, illuminated by migrating earthquake swarms. *Science Advances*, 4(8):eaat5258, 2018. doi: 10.1126/sciadv.aat5258.

Hunter, J. D. Matplotlib: A 2D Graphics Environment. *Computing in Science and Engineering*, 9(3):90–95, 2007. doi: 10.1109/MCSE.2007.55.

Hurst, A. W., Bibby, H. M., and Robinson, R. R. Earthquake focal mechanisms in the central Taupo Volcanic Zone and their relation to faulting and deformation. *New Zealand Journal of Geology and Geophysics*, 45(4):527–536, 2002. doi: 10.1080/00288306.2002.9514989.

Hurst, T., Bannister, S., Robinson, R., and Scott, B. Characteristics of three recent earthquake sequences in the Taupo Volcanic Zone, New Zealand. *Tectonophysics*, 452(1–4):17–28, 2008. doi: 10.1016/j.tecto.2008.01.017.

Husen, S. and Hardebeck, J. L. Theme IV - Understanding Seismicity Catalogs and their Problems : Earthquake Location Accuracy, 2010. doi: 10.5078/corssa-55815573.Available.

Illsley-Kemp, F., Herath, P., Chamberlain, C. J., Michailos, K., and Wilson, C. J. N. A decade of earthquake activity at Taupō Volcano, New Zealand. *Volcanica*, 5(2):335–348, 2022. doi: 10.30909/vol.05.02.335348.

Illsley-Kemp, F., Savage, M. K., Wilson, C. J. N., and Bannister, S. Mapping Stress and Structure From Subducting Slab to Magmatic Rift: Crustal Seismic Anisotropy of the North Island, New Zealand. *Geochemistry, Geophysics, Geosystems*, 20(11): 5038–5056, 2019. doi: 10.1029/2019GC008529.

Illsley-Kemp, F., Barker, S. J., Wilson, C. J. N., Chamberlain, C. J., Hreinsdóttir, S., Ellis, S., Hamling, I. J., Savage, M. K., Mestel, E. R. H., and Wadsworth, F. B. Volcanic Unrest at Taupō Volcano in 2019: Causes, Mechanisms and Implications. *Geochemistry, Geophysics, Geosystems*, 22(6), 2021. doi: 10.1029/2021GC009803.

Jónsson, S. Stress interaction between magma accumulation and trapdoor faulting on Sierra Negra volcano, Galápagos. *Tectonophysics*, 471(1–2):36–44, 2009. doi: 10.1016/j.tecto.2008.08.005.

Krischer, L., Megies, T., Barsch, R., Beyreuther, M., Lecocq, T., Caudron, C., and Wassermann, J. ObsPy: a bridge for seismology into the scientific Python ecosystem. *Computational Science and Discovery*, 8(1):1–17, 2015. doi: 10.1088/1749-4699/8/1/014003.

Langridge, R., Ries, W., Litchfield, N., Villamor, P., Van Dissen, R., Barrell, D., Rattenbury, M., Heron, D., Haubrock, S., Townsend, D., Lee, J., Berryman, K., Nicol, A., Cox, S., and Stirling, M. The New Zealand Active Faults Database. *New Zealand Journal of Geology and Geophysics*, 59(1):86–96, 2016. doi: 10.1080/00288306.2015.1112818.

Lomax, A., Virieux, J., Volant, P., and Berge, C. Probabilistic earthquake location in 3D and layered models: Introduction of a Metropolis-Gibbs method and comparison with linear locations, 2000.

MacQueen, J. Some methods for classification and analysis of multivariate observations. Proc. 5th Berkeley Symp. Math. Stat. Probab., Univ. Calif. 1965/66, 1, 281-297 (1967)., 1967.

McGregor, R. F. D., Illsley-Kemp, F., and Townend, J. The 2001 Taupō Fault Belt seismicity as evidence of magma-tectonic interaction at Taupō volcano. *Geochemistry, Geophysics, Geosystems*, 2022. doi: 10.1029/2022GC010625.

Miller, C. A. and Jolly, A. D. A model for developing best practice volcano monitoring: a combined threat assessment, consultation and network effectiveness approach. *Natural Hazards*, 71 (1):493–522, 2014. doi: 10.1007/s11069-013-0928-z.

Miller, C. A., Le Mével, H., Currenti, G., Williams-Jones, G., and Tikoff, B. Microgravity changes at the Laguna del Maule volcanic field: Magma-induced stress changes facilitate mass addition. *Journal of Geophysical Research: Solid Earth*, 122(4):3179–3196, 2017. doi: 10.1002/2017JB014048.

Newman, A., Dixon, T., Ofoegbu, G., and Dixon, J. Geodetic and seismic constraints on recent activity at Long Valley Caldera, California: evidence for viscoelastic rheology. *Journal of Volcanology and Geothermal Research*, 105(3):183–206, 2001. doi: 10.1016/S0377-0273(00)00255-9.

Otway, P. M., Illsley-Kemp, F., and Mestel, E. R. H. Taupō volcano's restless nature revealed by 42 years of deformation surveys, 1979–2021. *New Zealand Journal of Geology and Geophysics*, page 1–17, 2022. doi: 10.1080/00288306.2022.2089170.

Panning, M., Dreger, D., and Tkalčić, H. Near-source velocity structure and isotropic moment tensors: A case study of the Long Valley Caldera. *Geophysical Research Letters*, 28(9):1815–1818, 2001. doi: 10.1029/2000GL012389.

Pedregosa, F., Varoquaux, G., Gramfort, A., Michel, V., Thirion, B., Grisel, O., Blondel, M., Prettenhofer, P., Weiss, R., Dubourg, V., Vanderplas, J., Passos, A., Cournapeau, D., Brucher, M., Perrot, M., and Duchesnay, E. Scikit-learn: Machine Learning in Python. *Journal of Machine Learning Research*, 12:2825–2830, 2011.

Peltier, A., Hurst, T., Scott, B., and Cayol, V. Structures involved in the vertical deformation at Lake Taupo (New Zealand) between 1979 and 2007: New insights from numerical modelling. *Journal of Volcanology and Geothermal Research*, 181(3–4):173–184, 2009. doi: 10.1016/j.jvolgeores.2009.01.017.

Petersen, T., Gledhill, K., Chadwick, M., Gale, N. H., and Ristau, J. The New Zealand National Seismograph Network. *Seismological Research Letters*, 82(1):9–20, 2011. doi: 10.1785/gssrl.82.1.9.

Potter, S. H., Jolly, G. E., Neall, V. E., Johnston, D. M., and Scott, B. J. Communicating the status of volcanic activity: revising New Zealand's volcanic alert level system. *Journal of Applied Volcanology*, 3(1):13, 2014. doi: 10.1186/s13617-014-0013-7.

Potter, S. H., Scott, B. J., Jolly, G. E., Johnston, D. M., and Neall, V. E. A catalogue of caldera unrest at Taupo Volcanic Centre, New Zealand, using the Volcanic Unrest Index (VUI). *Bulletin of Volcanology*, 77(9):78, 2015. doi: 10.1007/s00445-015-0956-5.

Power, W., Roger, J., Gusman, A., Wang, X., Burbidge, D., Shanks, J., Rosenberg, M., Asher, C., Britten, K., Johnson, R., Moore, M., Moran, C., Brakenrig, T., Coup, L., Macdonald, N., and Krippner, J. Tsunamis in Lake Taupō, New Zealand on November the 30th 2022: observations, interpretation, and implications. Geoscience Society of New Zealand, 2023.

Ristau, J. Implementation of Routine Regional Moment Tensor Analysis in New Zealand. *Seismological Research Letters*, 79(3): 400–415, 2008. doi: 10.1785/gssrl.79.3.400.

Sandanbata, O., Watada, S., Satake, K., Kanamori, H., Rivera, L., and Zhan, Z. Sub-Decadal Volcanic Tsunamis Due To Submarine Trapdoor Faulting at Sumisu Caldera in the Izu–Bonin Arc. *Journal of Geophysical Research: Solid Earth*, 127(9), 2022. doi: 10.1029/2022JB024213.

Sandanbata, O., Watada, S., Satake, K., Kanamori, H., and Rivera, L. Two Volcanic Tsunami Events Caused by Trapdoor Faulting at a Submerged Caldera Near Curtis and Cheeseman Islands in the Kermadec Arc. *Geophysical Research Letters*, 50(7): e2022GL101086, 2023. doi: 10.1029/2022GL101086.

Saunders, S. J. The shallow plumbing system of Rabaul caldera: a partially intruded ring fault? *Bulletin of Volcanology*, 63(6): 406–420, 2001. doi: 10.1007/s004450100159.

Sherburn, S. Characteristics of earthquake sequences in the Central Volcanic Region, New Zealand. *New Zealand Journal of Geology and Geophysics*, 35(1):57–68, 1992. doi: 10.1080/00288306.1992.9514500.

Stagpoole, V., Miller, C., Caratori Tontini, F., Brakenrig, T., and Macdonald, N. A two million-year history of rifting and caldera volcanism imprinted in new gravity anomaly compilation of the Taupō Volcanic Zone, New Zealand. *New Zealand Journal of Geology and Geophysics*, 64(2–3):358–371, 2020. doi: 10.1080/00288306.2020.1848882.

Thorndike, R. L. Who belongs in the family? *Psychometrika*, 18(4): 267–276, 1953. doi: 10.1007/BF02289263.

Uieda, L., Tian, D., Leong, W. J., Schlitzer, W., Grund, M., Jones, M., Fröhlich, Y., Toney, L., Yao, J., Magen, Y., Tong, J.-H., Materna, K., Belem, A., Newton, T., Anant, A., Ziebarth, M., Quinn, J., and Wessel, P. PyGMT: A Python interface for the Generic Mapping Tools. doi: 10.5281/zenodo.7772533.

Utsu, T., Ogata, Y., S, R., and Matsu'ura. The Centenary of the Omori Formula for a Decay Law of Aftershock Activity. *Journal of Physics of the Earth*, 43(1):1–33, 1995. doi: 10.4294/jpe1952.43.1.

Vandergoes, M. J., Hogg, A. G., Lowe, D. J., Newnham, R. M., Denton, G. H., Southon, J., Barrell, D. J., Wilson, C. J., McGlone, M. S., Allan, A. S., Almond, P. C., Petchey, F., Dabell, K., Dieffenbacher-Krall, A. C., and Blaauw, M. A revised age for the Kawakawa/Oruanui tephra, a key marker for the Last Glacial Maximum in New Zealand. *Quaternary Science Reviews*, 74:195–201, 2013. doi: 10.1016/j.quascirev.2012.11.006.

Waite, G. P. and Smith, R. B. Seismic evidence for fluid migration accompanying subsidence of the Yellowstone caldera. *Journal of Geophysical Research: Solid Earth*, 107(B9):ESE 1–1–ESE 1–15, 2002. doi: 10.1029/2001JB000586.

Waldhauser, F. and Ellsworth, W. L. A Double-Difference Earthquake Location Algorithm: Method and Application to the Northern Hayward Fault, California. *Bulletin of the Seismological Society of America*, 90(6):1353–1368, 2000. doi: 10.1785/0120000006.

Wiemer, S. and Wyss, M. Minimum Magnitude of Completeness in Earthquake Catalogs: Examples from Alaska, the Western United States, and Japan. *Bulletin of the Seismological Society of America*, 90(4):859–869, 2000. doi: 10.1785/0119990114.

Wiemer, S., McNutt, S. R., and Wyss, M. Temporal and three-dimensional spatial analyses of the frequency-magnitude distribution near Long Valley Caldera, California: The frequency-magnitude distribution near Long Valley. *Geophysical Journal International*, 134(2):409–421, 1998. doi: 10.1046/j.1365-246x.1998.00561.x.

Wilson, C. The 26.5 ka Oruanui eruption, New Zealand: an introduction and overview. *Journal of Volcanology and Geothermal Research*, 112(1–4):133–174, 2001. doi: 10.1016/S0377-0273(01)00239-6.

Wilson, C. J. N. Stratigraphy, chronology, styles and dynamics of late Quaternary eruptions from Taupo volcano, New Zealand. *Philosophical Transactions of the Royal Society of London. Series A: Physical and Engineering Sciences*, 343(1668):205–306, 1993. doi: 10.1098/rsta.1993.0050.

Wyss, M., Shimazaki, K., and Wiemer, S. Mapping active magma chambers by b values beneath the off-Ito volcano, Japan. *Journal of Geophysical Research: Solid Earth*, 102(B9):20413–20422, 1997. doi: 10.1029/97JB01074.

Zhan, Y., Gregg, P. M., Le Mével, H., Miller, C. A., and Cardona, C. Integrating Reservoir Dynamics, Crustal Stress, and Geophysical Observations of the Laguna del Maule Magmatic System by FEM Models and Data Assimilation. *Journal of Geophysical Research: Solid Earth*, 124(12):13547–13562, 2019. doi: 10.1029/2019JB018681.

Zhang, H. and Thurber, C. Double-difference tomography: The method and its application to the Hayward Fault, California. *Bulletin of the Seismological Society of America*, 93(5): 1875–1889, 2003. doi: 10.1785/0120020190.